Seizures, spreading depolarizations and sudden death

Jansen, N.A.

Chapter 3

Spontaneous spreading depolarizations originate subcortically in a novel mouse model of familial hemiplegic migraine type 2

Nico A. Jansen
Chelsey Linnenbank
Maarten Schenke
Rob A. Voskuyl
Maria S. Jorge
Georgii Krivoshein
Cor Breukel
Margot M. Linssen
Jill W.C. Claassens
Conny Brouwers
Sandra H. van Heiningen
Anders Heuck
Karin Lykke-Hartmann
Else A. Tolner
Arn M.J.M. van den Maagdenberg

Neurobiol Dis 2024;202:106714

ABSTRACT

The mechanisms of initiation of spreading depolarization (SD) are understudied due to a paucity of disease models with spontaneously occurring events. We here present a novel mouse model of familial hemiplegic migraine type 2 (FHM2), expressing the missense T345A-mutated a2 subunit of the Na^+/K^+ adenosine triphosphatase pump (*Atp1a2*^{T345A}). Homozygous *Atp1a2*^{T345A} mice showed regular spontaneous SDs that exhibit a diurnal rhythm and typically originate from the hippocampus. Heterozygous *Atp1a2*^{T345A} mice rarely exhibited spontaneous SDs and, for electrically induced SDs, only showed an increased propagation speed, whereas homozygotes showed both increased propagation and decreased threshold. Remarkably, despite hippocampal hyperexcitability, spontaneous SDs in *Atp1a2*^{T345A} mice were only rarely associated with epileptic behavior, and seizure expression during kindling was decreased. Spontaneous SDs could be prevented by modulation of persistent sodium currents. Hippocampal SDs occurred in the presence of an NMDA-receptor antagonist, but these events did not reach the cortex, suggesting that initiation and propagation of SD depend on different mechanisms in this model.

INTRODUCTION

Spreading depolarization (SD) is an electrophysiological phenomenon characterized by prolonged depolarization of brain cells that propagates through grey matter, followed by depression of neuronal activity that lasts for minutes.[1] Cortical SD is considered the neurophysiological phenomenon underlying the migraine aura, a transient focal symptom that precedes headache in one-third of migraine patients.[2] Although different triggers can initiate SD under experimental conditions, a paucity of models of spontaneous SD limits our understanding and treatment of this phenomenon.

Familial hemiplegic migraine type 2 (FHM2) is a rare subtype of migraine with severe auras caused by loss-of-function mutations in the *ATP1A2* gene.[3] *ATP1A2* encodes the α2 subunit of the Na^+/K^+ adenosine triphosphatase (α_2NKA), which acts as a Na^+/K^+-ATPase pump that in adult mice is predominantly expressed in astrocytes.[4] Loss of α_2NKA function has previously been studied in heterozygous knock-in mice expressing missense mutations W887R and G301R. Both *Atp1a2*^{W887R} [5] and *Atp1a2*^{G301R} mice[6] show increased susceptibility to experimentally induced cortical SD, which in *Atp1a2*^{W887R} mice was found associated with a reduced rate of K^+ and glutamate clearance by cortical astrocytes.[7] Of note, also *Atp1a2*$^{+/-}$ mice showed an increased susceptibility to cortical SD[8], although this was not confirmed in another study that showed only a tendency for increased propagation when SDs were evoked under anesthesia.[9]

Notably, homozygous FHM2 mutant mice of the various strains that lack expression of α_2NKA die at or around birth,[5] similar to *Atp1a2*$^{-/-}$ mice that die due to absent respiratory activity immediately after birth.[10] In rare clinical cases of *ATP1A2* homozygous loss-of-function mutations, the absence of α_2NKA protein also led to respiratory distress immediately after birth and subsequent death.[11, 12]

In contrast to FHM2 mutations that lead to absence of α_2NKA protein, the FHM2 *ATP1A2* T345A missense mutation was suggested to result in a decreased affinity for K^+ to mutated Na^+/K^+-ATPase pumps in some,[13] but not all[14, 15] cellular heterologous overexpression studies. Such discrepancy seems due to inherent difficulties with such studies that also produced inconsistent results for other FHM2 mutations. Regardless, the T345A mutation seems to mildly affect Na^+/K^+ ATPase function, compared to the W887R[16] and G301R[17] mutations. Here we generated heterozygous and homozygous *Atp1a2*^{T345A} mice to study *in vivo* effects of the T345A mutation on brain function. We found that homozygous *Atp1a2*^{T345A} mice were viable and had no apparent impairment of mobility, but showed decreased survival and increased susceptibility to cortically induced SD. Moreover, spontaneous cortical SD events occurred in homozygous mutants, with remarkably regular intervals and consistent propagation from visual to motor cortex, and typically originated from the hippocampus. In heterozygous mutants, spontaneous SDs were rarely observed, whereas no such events occurred in wildtype mice. Electrical stimulation of the hippocampus in homozygous mutants resulted in SD that propagated to cortical regions, but, in contrast to wildtype mice, repeated stimulation (i.e., kindling) did not result in the development of seizures. Finally, initiation of spontaneous SD in *Atp1a2*^{T345A} mice was modulated by a preferential inhibitor of persistent

sodium currents. An NMDA receptor (NMDAR) antagonist failed to prevent hippocampal SDs, but effectively blocked propagation to the cortex, suggesting different mechanisms for initiation and propagation of spontaneous SDs in this model. Our findings indicate that spontaneous SDs in the *Atp1a2*^{T345A} mouse model originate from the hippocampus, with demonstrable consequences for strategies to prevent SD.

MATERIALS AND METHODS

Generation of *Atp1a2*^{T345A} mice

A 12 kb targeting construct containing a loxP-PGK-Neo-pA-loxP cassette in intron 8 harboring the human FHM2 T345A missense mutation in exon 9 (Fig. 1A) was used as template for CRISPR/Cas9-mediated homologous recombination, and was introduced in JM8N4 (subcloned from JM8 parental line derived from C57BL/6N[18]) embryonic stem cells by electroporation of the DNA construct and the pX459 plasmid containing cas9 and the CRISPR guide sequence (Int8): aactgtcgctatttcctgct. The obtained embryonic stem cell clones were analyzed, selected for homologous recombination and correct karyotype after which the targeted JM8 ES cells were injected into a C57BL/6J mouse background. Obtained male chimeras were bred to C57BL/6J females to achieve germline transmission. To remove the Neo cassette, mice of the F1 generation were crossed to Cre-deleter mice (strain: B6.Cg-Tg(EIIa-cre)C5379Lmgd/Jlumc; the Jackson Laboratory, Stock number 003724). For further maintenance breeding, C57BL/6J mice were used. Male and female heterozygous and homozygous *Atp1a2*^{T345A} mice and wildtype (WT) littermates were used for the experiments. Mice were kept under standard housing conditions (temperature of 22 ± 1.5 °C, 12-h light/12-h dark cycle) with free access to water and food. Experiments were approved by the local and national ethical committees according to ARRIVE guidelines and recommendations of the European Communities Council Directive (2010/63/EU). All efforts were made to minimize discomfort of experimental animals.

Western blot analysis

Fresh brain tissue isolation of the right hemisphere of 1.5- to 2-month-old WT, heterozygous and homozygous *Atp1a2*^{T345A} mice was performed on ice. Tissues were homogenized in ice-cold lysis buffer, containing 1% sodium dodecylsulfate (SDS), 1 mM Na_3VO_4, protease inhibitor cocktail (cOmplete, mini, EDTA-free) and 10 mM Tris (pH 7.4) using a MagNalyzer (Roche Diagnostics, Almere, the Netherlands) for 20 s at 7000 rpm. Lysates were centrifuged for 2 min at 1000 g at 4 °C and supernatant was stored at -80 °C until western blot analysis. Protein expression was analyzed by TruPage on 4-12% precast gels in MOPS running buffer, followed by wet transfer to PVDF membranes. Membranes were blocked in 5% porcine serum in PBS-T and probed with primary antibody mouse anti-α1 Na^+/K^+ ATPase (1:60, a6F; Developmental Studies Hybridoma Bank, Iowa City, IA, USA), rabbit anti-α2 Na^+/K^+ ATPase (1:500; 07–674; Millipore, Burlington, MA, USA)

or mouse anti-β-Actin (1:5000, A5441; Sigma-Aldrich, St. Louis, MO, USA) diluted 1:1 in PBS-T blocking buffer. Primary antibodies were detected using HRP-conjugated secondary antibody (Li-Cor Biosciences, Lincoln, NE, USA) and ECL reaction with ImageQuant LAS400 mini system (GE Healthcare Bio-Sciences AB, Uppsala, Sweden).

Immunohistochemistry

Mice were perfused with PBS and 4% PFA. Brains were post-fixed for 2 h, followed by a serial incubation in 10% and 30% sucrose (each 12 h) for cryoprotection, and frozen in OCT tissue freezing medium (Tissue-Tek; Sakura Finetek, Los Angeles, CA, USA). Tissues were coronally sectioned at 10-µm thickness on a cryostat. Prior to staining, slides were heated in 10 mM citrate buffer (pH 6.0) for antigen retrieval and sections were permeabilized with 1% Triton X-100. Sections were then incubated with blocking serum (10% normal horse serum in PBS containing 0.05% Triton X-100) for 60 min and followed by double labelling with rabbit anti-a2 Na^+/K^+ ATPase (1:200, 07-674; Millipore) or chicken anti-GFAP (1:500, ab134014; Abcam, Cambridge, UK) antibody overnight at 4 ^{0}C in PBS with 2% normal horse serum and 0.4% Triton X-100. Incubation with secondary antibody Alexa 647 goat anti-rabbit (1:200, A21245; Invitrogen, Waltham, MA, USA) or Alexa 488 donkey anti-chicken (1:200, 703-545-155; Jackson ImmunoResearch, West Grove, PA, USA) was performed for 2 h. Sections were cover slipped in Vectashield hard mounting medium (Vectorlabs, Newark, NJ, USA) containing 1 µL/mL Hoechst-33258 and examined by confocal SP8 microscopy.

Pathology

For pathological examination, various tissues (including brain, muscle, heart and lung) were collected from 1.5- to 2-month-old WT, heterozygous and homozygous *Atp1a2*^{T345A} mice. Tissues were freshly isolated and post-fixed and processed for paraffin-sectioning or frozen for cryosectioning, followed by hematoxyline-eosine staining.

Surgery

For recordings of spontaneous brain activity, animals (postnatal (P) 32-50) were implanted with local field potential (LFP) electrodes (75 µm platinum/iridium; PT6718; Advent Research Materials, Oxford, UK) under isoflurane anaesthesia (induction 4%; maintenance 1.5%). Four electrode configurations were used (in mm relative to bregma, anterior/lateral/ventral, respectively): (1) bilateral primary motor cortex (M1; 1.5/1.8/0.5) and primary visual cortex (V1; -3.5/2.4/0.5); (2) right M1, V1, caudal V1 (V1c; -4.2/2.4/0.5) and dorsal hippocampus (dHC; -2.5/2.0/1.2), and for a subset of mice also ventral hippocampus (vHC; -2.8/2.8/2.6); (3) right M1, V1, and caudal, medial (-3.5/1.1/0.5) and lateral (-3.5/3.7/0.5) to V1; and (4) for recordings of respiratory functioning, a subset of animals were also equipped with a thermistor probe (MEAS-G22K7MCD419, Measurement Specialties Inc., Hampton, VA, USA) inserted in a hollow space overlying the epithelium of the anterior nasal cavity, as described previously,[19] in addition to a silver ball tip electrode (75 µm, AG5493; Advent Research Materials) on the dura overlying V1. For cortical SD electrical threshold

experiments, a separate group of 2- to 4-month-old WT and homozygous *Atp1a2*^{T345A} mice was implanted under isoflurane anesthesia with bipolar stimulation electrodes in bilateral caudal V1 (-3.8/2.3/0.5), with recording electrodes in bilateral rostral V1 (-2.5/2.4/0.5), M1, and the right dorsal HC (-2.2/1.5/1.7). In the latter experiments an additional 400-µm diameter laser doppler probe (403 probe and Periflux System 5000, Perimed Järfälla-Stockholm, Stockholm, Sweden) was placed bilaterally on the parietal skull (-1.5/2/0).

Cortical SD threshold assessment

For cortical SD induction in freely behaving mice, two stimulations were performed per animal (once in each hemisphere) one week after surgery with at least a 24-h interval. Cathodal pulses of increasing intensities (1–5000 µC) were delivered every 3 min until a cortical SD was observed, similar as reported previously,[20] and the propagation speed between electrodes in V1 and M1 was calculated. The additional laser doppler signal served to confirm spread of SD in case of technical issues with one of the direct current (DC)-recordings.

Hippocampal kindling

For hippocampal kindling experiments, a bipolar stimulation electrode was implanted in the left ventral hippocampal CA3 region (-3.0/3.0/2.8) in 2- to 4-month-old animals. Unipolar electrodes were implanted in right dorsal CA3, CA1 (-2.5/2.0/1.2) and V1. Following one day of baseline recording, a train of 1-ms bipolar current pulses (60 Hz for 2 s) was delivered through the hippocampal CA3 electrode every 5 min with increasing current intensities (10-µA steps), until afterdischarges (ADs) lasting ≥5 s were observed. This current intensity was used to trigger ADs twice daily (8-9 AM and 6-8 PM) for the subsequent 15 days. The first hippocampal stimulation session was used for comparing evoked SD features between dorsal CA3 and CA1.

Pharmacology

To test for possible effects of NMDA antagonism on spontaneous events, homozygous *Atp1a2*^{T345A} mice received intraperitoneal injections of either MK-801 (Sigma-Aldrich; 0.5 mg/kg body weight) or vehicle twice daily (8 A.M. and 6 P.M.) for three days, followed by the other treatment, by an experimenter blinded to the treatment. In a second group of homozygous *Atp1a2*^{T345A} mice, the effect of the sodium channel modulator GS967 (also known as PRAX-330) on spontaneous events was tested. Following a baseline recording period of one week, standard chow was replaced by chow containing 8 mg/kg GS967 (Research diets Inc., New Brunswick, NJ, USA), a dose that was previously shown to not cause overt behavioral effects.[21] After one week, GS967-compounded chow was replaced with standard chow for an additional recording period of one week.

Data acquisition and analyses

Wildtype, heterozygous and homozygous *Atp1a2*^{T345A} mice were videotaped at age P24-P54 in a PhenoTyper cage (Model 3000, Noldus Information Technology, Wageningen, the Netherlands) for 24 h. For tracking, mice were placed in the cage between 2:00 PM-4:00 PM. Video tracking and analysis of locomotor activity was performed offline using EthoVision software (Ethovision XT version 11.5, Noldus Information Technology). Locomotor activity was assessed in 1-h time bins and analyzed for the 12th h (i.e., dark period) and 24th h (i.e., light period) by determining total distance moved and mean velocity.

Animals that received surgery were allowed to recover for at least 2 days (for recordings of spontaneous activity) or 7 days (for cortical or hippocampal stimulation), after which they were connected to a 7-channel commutator in a Faraday cage for continuous recording of video, LFP and/or respiratory activity. Data were acquired and digitized as described previously.[22]

For power spectral density (PSD) analyses, alternating current (AC) LFP was artefact-rejected, digitally lowpass filtered (Chebyshev IIR 8th-order filter) and down-sampled to 500 Hz. PSD between 2-100 Hz was calculated using a fast Fourier transform with a Hamming window of 1 s with 50% overlap, and normalized to the average PSD within this range in the 30 s preceding stimulation (pre-stimulus). For post hoc assessment of AD duration, the time the PSD remained 2 (for hippocampus) or 1.5 (for V1) times above pre-stimulus total power was used. For V1 LFP, the reference signal and data from an infrared motion detection sensor were analyzed per 5-s epoch to establish the animal's vigilance state, for a 24-h period starting 7 days after surgery. Epochs without locomotor activity or motion artefacts were considered NREM or REM sleep based on V1 LFP PSD: epochs with a theta (5 – 10 Hz) to delta (1 – 4 Hz) power ratio of >2.5 were defined as REM sleep, while epochs with a high delta power were defined as NREM sleep. Analyses were performed using custom-written MATLAB scripts (version 2019b, Mathworks, Cambridge, UK).

For spontaneous SDs, video-recorded behavior was analyzed before and after the start of the event (i.e., the start of the burst or the start of the DC shift in case of an SD without prior burst activity) using Observer software (Observer XT version 15). Detection of burst activity required the burst amplitude to exceed 2X the value of the averaged root mean square of baseline LFP.

Statistical analysis

Data are presented as mean ± SEM (for time series) or mean ± SD (other). Statistical testing was performed in MATLAB or Graphpad Prism (Graphpad Software, San Diego, CA, USA). Data were compared using a Wilcoxon signed-rank or Mann-Whitney U test for single comparisons. For multiple comparisons, dependent on a prior analysis whether data were normally distributed, a two-way ANOVA, Kruskal-Wallis, Brown-Forsythe, or Welch's ANOVA test was used, followed by a post hoc Tukey's test or unpaired *t*-test with Welch's correction.

RESULTS

Generation of homozygous *Atp1a2*^{T345A} mice and expression of the Na^+/K^+-ATPase α2 subunit

CRISPR/Cas9-mediated homologous recombination was used to successfully introduce the human FHM2 T345A missense mutation in exon 9 of the orthologous mouse *Atp1a2* gene, generating heterozygous and homozygous *Atp1a2*^{T345A} mice (Fig. 1A-C). Western blot quantification of the α1 and α2 isoforms showed expression of both isoforms in the brains of *Atp1a2*^{T345A} and WT mice (Fig. 1D). Immunofluorescence revealed astrocytic expression of the Na^+/K^+-ATPase α2 subunit in hippocampal neurons of *Atp1a2*^{T345A} mice and WT mice (Fig. 1E). Pathological macroscopic and microscopic examination of brain, muscle (gastrocnemius and masseter), heart and various other tissues (lung and diaphragm, liver, spleen, kidney, adrenal gland and thymus) of *Atp1a2*^{T345A} mice revealed no overt abnormalities.

Homozygous *Atp1a2*^{T345A} mice are viable and show an increased susceptibility to cortical SD

In contrast to other FHM2 knock-in models[5, 23] homozygous *Atp1a2*^{T345A} mice were viable, although animals died prematurely from postnatal week 3 onwards (Fig. 2A). Despite early mortality, the animals had a normal appearance, albeit with a reduction in body weight and size that was evident throughout development into adulthood (Supplementary Fig. S1 A-C). Gross behavioral activity of homozygous *Atp1a2*^{T345A} mice seemed unimpaired, as evidenced by total distance moved and mean velocity (Supplementary Fig. S1 D-F).

To study the effects of the mutation on SD susceptibility, we assessed the threshold and propagation speed of induced cortical SD in WT, heterozygous and homozygous *Atp1a2*^{T345A} mice. Following cortical electrical stimulation, homozygous mutants showed a decreased threshold (Fig. 2B) and an increased propagation speed of SD (Fig. 2C) when compared to WT mice. SD propagation speed, but not electrical threshold, was significantly affected in heterozygous mutants compared to WT animals (Fig. 2B and 2C). DC shift duration of the evoked cortical SDs did not differ between homozygous *Atp1a2*^{T345A} mutants (67.1 ± 8.3 seconds; $n = 6$), heterozygous *Atp1a2*^{T345A} mutants (59.8 ± 4.7 seconds; $n = 13$) and wildtype mice (48.9 ± 4.7 seconds; $n = 10$; $p = 0.12$; Kruskal-Wallis test).

FIGURE 1A-1D. Generation, molecular characterization, and α2NKA expression in knock-in (KI) *Atp1a2*^{T345A} mice.

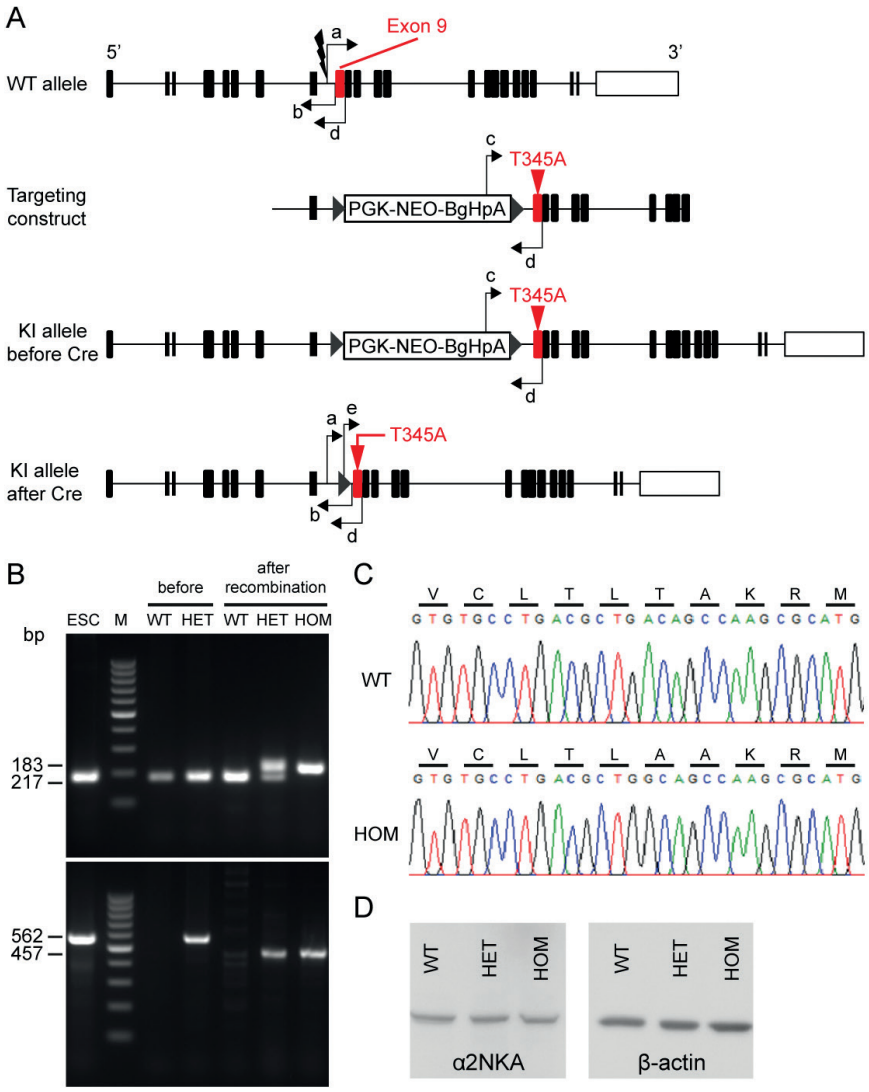

(A) Genomic structure of the wildtype (WT) *Atp1a2* allele, targeting construct containing a loxP-PGK-Neo-pA-loxP cassette (PGK-NEO-BgHpA) in intron 8, structure of the KI allele after homologous recombination (KI allele before Cre), and after Cre-mediated deletion of the cassette (KI allele after Cre). For introduction of the T345A missense mutation in exon 9 (red), a targeting construct combined with a Cas9 containing plasmid and the Crispr guide sequence were used. Positions and direction of the primers used to verify correct targeting of the T345A mutation are indicated by arrows. Sequences of the primers: a: 5'-ctttcttccgggcgtttacc-3'; b: 5'-aaaagggccaagtcgagagt-3', c: 5'-gacagcaaggggaggattg-3'; d: 5'-gagcatttcataccccagga-3'; and e: 5'-gctatttcctgctagataattcg-3'. **(B)** PCR products for primer combinations ab (183 bp (WT allele and before Cre recombination) and 217 bp (after Cre recombination)), cd (562 bp (before Cre recombination), and ed (457 bp after recombination)). **(C)** Sequencing analysis of RT-PCR product of hippocampus of WT and homozygous *Atp1a2*^{T345A} (HOM) mice. **(D)** Western blot of brain (cortex) protein lysate isolated from WT, heterozygous *Atp1a2*^{T345A} (HET) and HOM mice probed for a2NKA (~100 KDa) or β-actin (~42 KDa) protein shows equal expression levels of a2NKA protein in all three genotypes.

FIGURE 1E. Generation, molecular characterization, and α2NKA expression in knock-in (KI) *Atp1a2*^{T345A} mice.

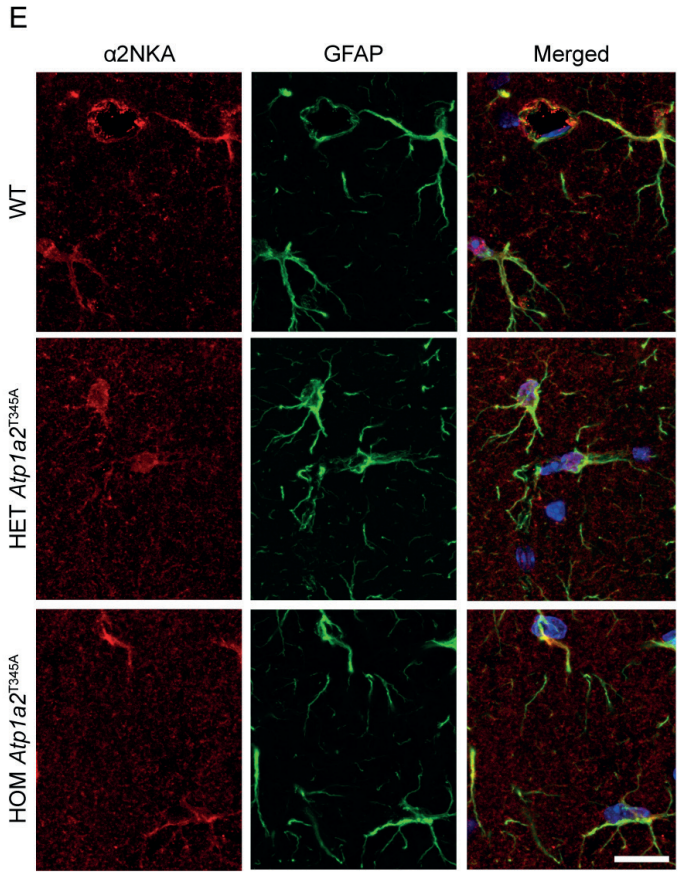

(E) Representative fluorescent images from hippocampal sections of WT, HET and HOM mice showing similar expression of 2NKA (red) in astrocytes stained with GFAP (green). Scale bar: 25 µm.

FIGURE 2. Decreased survival and reduced threshold and increased propagation speed for cortical SD induced by electrical stimulation in *Atp1a2*^{T345A} mice.

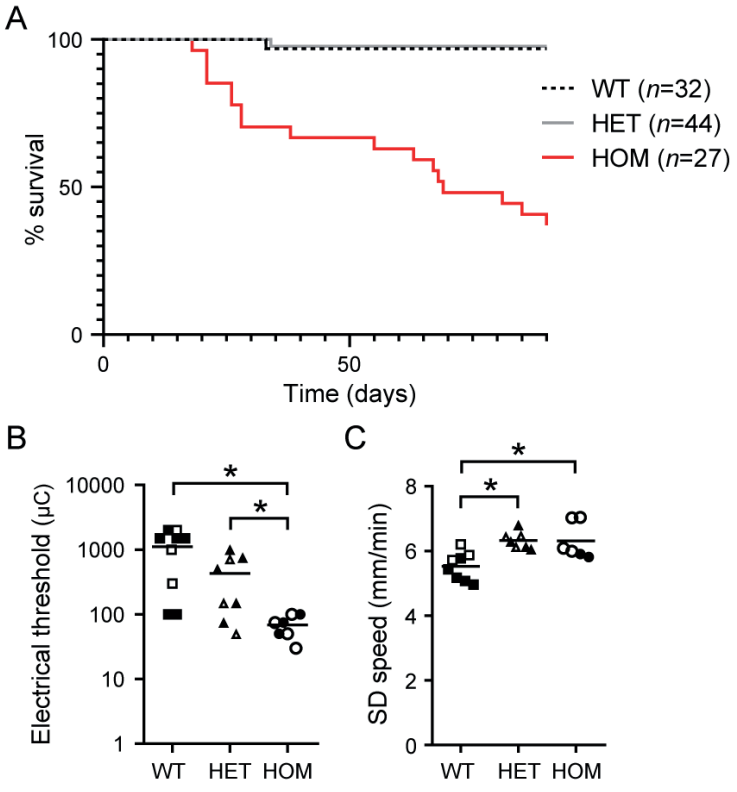

(A) Early mortality occurred from the 3rd postnatal week in homozygous *Atp1a2*^{T345A} mice. Survival was significantly decreased in homozygous *Atp1a2*^{T345A} compared to heterozygous *Atp1a2*^{T345A} and WT mice ($p < 0.001$, Log-rank test). **(B, C)** Electrical stimulation in the right and left hemisphere (closed and open symbols, respectively) resulted in significantly different SD thresholds (B; $p = 0.0004$ and 0.0499 for HOM vs WT and HET, respectively, Kruskal-Wallis and post-hoc Dunn's test) and propagation speeds between V1 and M1 cortex (C; $p = 0.0020$ and 0.0221 for HET and HOM vs WT, respectively, Kruskal-Wallis and post-hoc Dunn's test) in WT ($n = 6$; 9 experiments), HET ($n = 5$; 8 experiments) and HOM ($n = 5$; 7 experiments) *Atp1a2*^{T345A} mice ($n = 6$; 9 experiments). Analyses concern grouped SD data from both hemispheres. For 1 experiment in all genotypes, propagation rate could not be reliably measured due to instability of 1 of the two DC channels.

Homozygous *Atp1a2*^{T345A} mice show abnormal behavior immediately prior to apnea-associated death

To investigate possible causes for the early mortality in homozygous *Atp1a2*^{T345A} mice, five mice were continuously videotaped from P24 onwards, which revealed apparent normal behavior in the hours before death. However, in the seconds preceding terminal behavioral immobility, tonic extension of the hindlimbs occurred, which was preceded by a running bout of 1 – 3 s duration in three animals. In addition, handling of homozygous *Atp1a2*^{T345A} mice occasionally resulted in sudden hindlimb extension and behavioral immobility (6 such events were recorded in the (repetitive) handling of 49 homozygous *Atp1a2*^{T345A} mice) from which some animals did not recover. Recordings of video-encephalography (EEG) and respiratory activity showed that sudden apnea occurred during spontaneous and provoked events (n = 5; example in Fig. 3). In two events respiratory activity did not restore leading to the death of the animal. During one of the events moderate amplitude epileptiform bursts were observed in the EEG. This epileptiform activity had no clear behavioral correlate and continued after terminal behavioral arrest (Fig. 3B). Contamination of the EEG by cardiac electrical activity could still be observed minutes after apnea onset (Fig. 3C). These data indicate that homozygous *Atp1a2*^{T345A} mice are viable, but show early mortality that appears mediated by sudden apnea.

FIGURE 3. Non-fatal and fatal sudden apnea in homozygous *Atp1a2*^{T345A} mice.

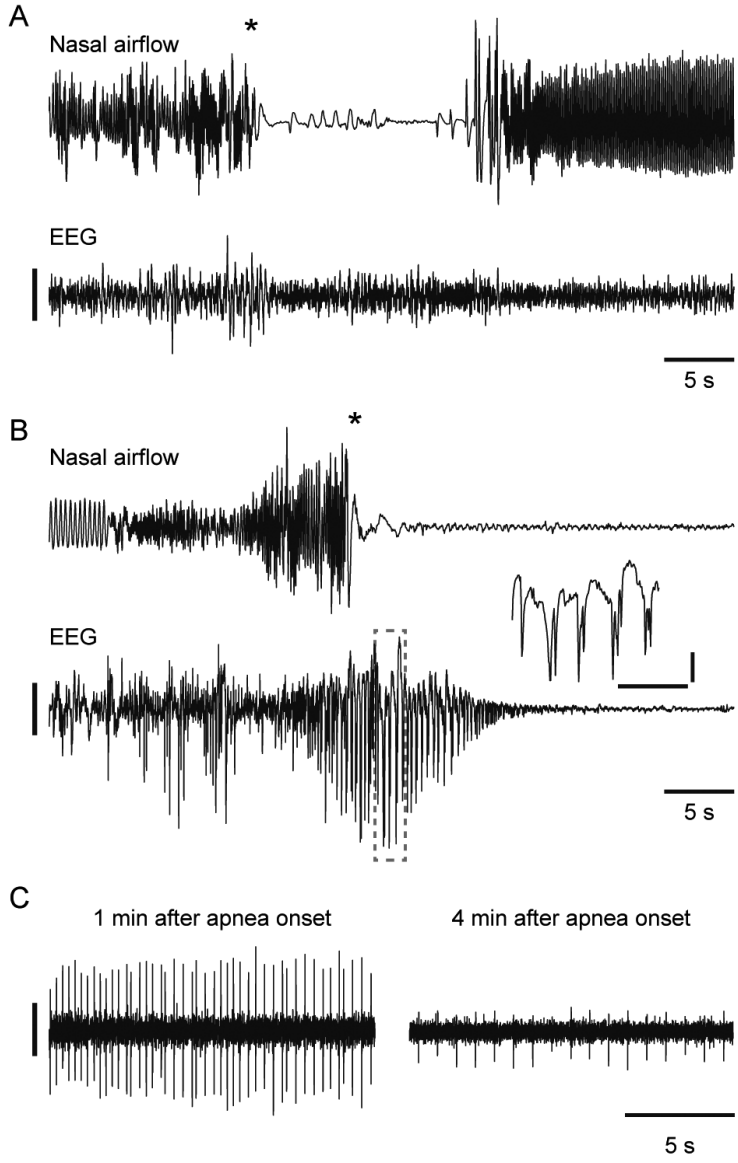

(A) Example of an episode of sudden non-fatal apnea in a homozygous *Atp1a2*^{T345A} mouse, that lasted ~15 s. Onset of apnea coincided with stretching of the hindlimbs (asterisk). The EEG, recorded from primary visual cortex, showed no epileptiform activity. **(B)** Example trace of sudden lethal apnea in a homozygous *Atp1a2*^{T345A} mouse. The EEG showed epileptiform bursts of moderate amplitude (detailed in inset, horizontal scale bar indicating 1 s) that initiated prior to apnea onset, but that had no behavioral correlate. **(C)** Contamination of the near-isoelectric EEG signal by ECG activity showed that cardiac activity was still present minutes after apnea onset. Digital filtering was performed with a highpass filter of 0.5 Hz (for EEG, in A and B) and with a bandpass filter of 10-500 Hz (for ECG, in C). Vertical scale bars indicate 0.5 mV (in A and B) and 20 μV (in C).

Atp1a2^{T345A} mice show spontaneous spreading depolarizations that typically originate from the hippocampus

In other FHM2 knock-in models[5, 23] no spontaneous SDs were reported in heterozygous mutants whereas homozygous mutants could not be investigated due to perinatal death. Here, we were able to record cortical LFP in homozygous *Atp1a2*^{T345A} mice (n = 3) continuously for 7 days, as these mice survive well past weaning (Fig. 4). Spontaneous SDs in the cortex were observed in all 3 animals, and in total 13 SDs were detected (range 3 – 6 SDs per animal). SDs exclusively propagated from V1 to M1 (example in Fig. 4A-C), and the time between SDs ranged from 8 – 51 hrs. Strikingly, in 8 of 13 events, cortical SDs were detected in both hemispheres almost simultaneously: the absolute delay between SD onset in left and right V1 was 13.0 ± 6.3 s, suggesting either a common subcortical source and/or synchronizing activity underlying SD onset. Inspection of LFP revealed epileptiform bursts of moderate amplitude and 20- to 30-s duration that were visible in both V1 and M1, and preceded V1 SD onset by 71 – 101 s.

We hypothesized that the hippocampus may represent a common source for the observed burst activity that preceded cortical SD. To study this, we implanted 19 homozygous *Atp1a2*^{T345A} mice with electrodes in the cortex, dorsal and, for a subset of mice (n = 12/19) also ventral hippocampus, and continuously recorded LFP for a total duration of 162.4 days, averaging 8.6 ± 5.4 (range 2 – 20) days per animal. In total, 1 – 26 SDs were observed per animal, totaling 149 SDs. For one event, the SD was first detected in the cortex, but the remaining 148 SDs were first observed in the hippocampus. Hippocampal LFP showed burst activity directly preceding SD in 90% (134/149) of the events (example in Supplementary Fig. S2), whereas no such abnormal activity was observed for the other 15 events. High-amplitude spikes in the hippocampal LFP occurred synchronously with lower amplitude spikes in cortical LFP, suggesting electric field transmission. The majority of hippocampal SDs (79%; 117/148) propagated to the uni- or bilateral cortex, from V1 to M1 (example in Fig. 4D), with a cortical propagation speed of 5.3 ± 0.5 (range 2.9 – 7.7) mm/min. Additional LFP recordings from different positions relative to V1 (Fig. 4E) confirmed that SDs propagated in a caudal-to-rostral pattern (Fig. 4F). Bilateral neocortical LFP was available during 52% of the events (77/149), allowing confirmation of bilateral, unilateral, or absence of, neocortical SD (Table 1). Hippocampal SD always occurred bilaterally preceding bilateral neocortical SD (39/39). For unilateral events, hippocampal and neocortical SD always occurred ipsilateral (7/7). These data indicate that cortical SDs in homozygous *Atp1a2*^{T345A} mice have a predominant hippocampal origin, with a cortical caudal to rostral propagation pattern. Propagation speed of spontaneous cortical SDs did not differ from that of the above-described induced SD events (p = 0.11).

Recordings of local oxygen partial pressure (PO_2) in the hippocampus of homozygous *Atp1a2*^{T345A} mice (n = 2, 6 spontaneous SD events) showed local hippocampal PO_2 of 21.4 ± 5.3 (range 17.2 – 30.1) mmHg at the time of SD onset (Supplementary Figure S3), mostly within ranges previously reported as "normoxic" for hippocampal recordings [24]. PO_2 starts decreasing during the hippocampal burst activity, but only reaches severe hypoxia (< 10 mm Hg PO_2) after SD onset,

indicating that neuronal activity causes local tissue hypoxia in homozygous *Atp1a2*^{T345A} mice, rather than vice versa.

Long-term hippocampal and cortical recordings in 8 heterozygous *Atp1a2*^{T345A} mice for a total duration of 52 days (6.5 ± 2.3 (range 2 – 9) days per animal) revealed two spontaneous SDs, detected in two animals. One event was preceded by hippocampal burst activity, followed by hippocampal and cortical SD spreading from V1 to M1, similar to homozygous mutants. The other event did not involve the hippocampus, but spread unilaterally from V1 to M1.

FIGURE 4. Cortical SDs occur spontaneously in homozygous *Atp1a2*^{T345A} mice and display a stereotypical spreading pattern.

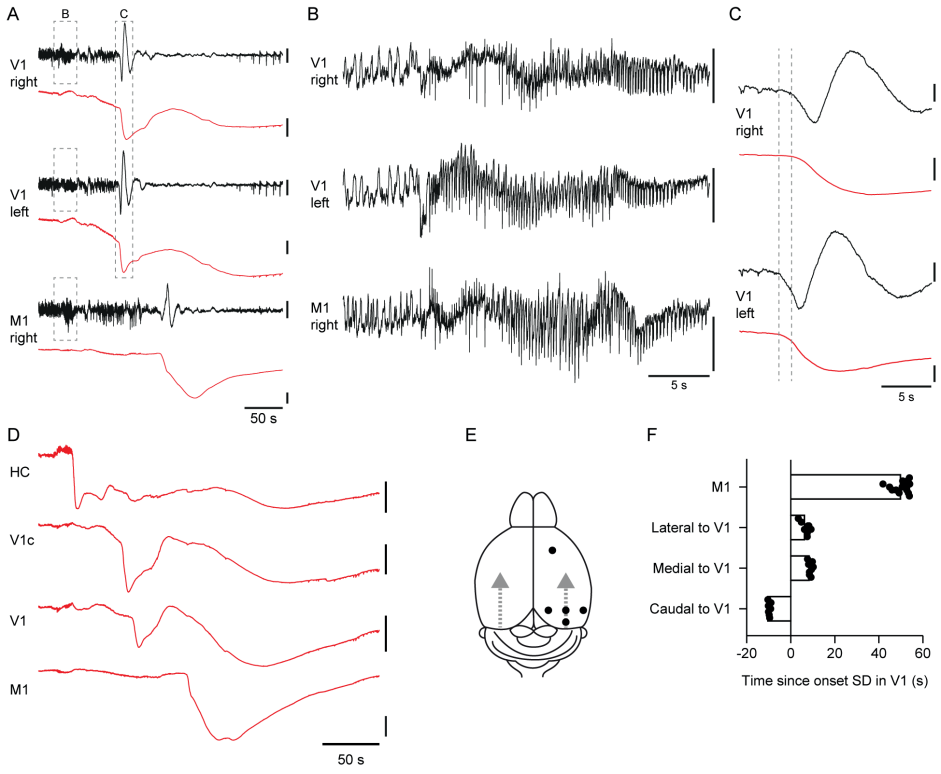

(A) Example of a spontaneous cortical SD in a homozygous *Atp1a2*^{T345A} mouse, with alternating current (AC) signals in black and direct current (DC) LFP signals in red. Vertical scale bars indicate 0.5 and 10 mV for AC and DC signals, respectively. **(B)** A synchronized burst of activity of moderate amplitude (inset from A) occurred approximately 74 s prior to SD onset in the primary visual cortex (V1). **(C)** Cortical SD onset was not synchronous in V1 of both hemispheres (inset from A), since the DC shift in left V1 preceded that in right V1 by approximately 1 s (dashed lines indicate SD onset). **(D)** Typical DC signals recorded from one hemisphere in a homozygous *Atp1a2*^{T345A} mouse during a spontaneous SD event with DC shifts occurring sequentially in hippocampus (HC), caudal V1 (V1c), V1, and primary motor cortex (M1). **(E)** Schematic of the neocortical sites recorded during spontaneous SD events, using three electrode configurations (described in the Materials and Methods). **(F)** SD timings in these areas indicated a caudal-to-rostral spreading pattern.

TABLE 1. Fraction of events that showed SD and/or hippocampal burst activity in homozygous *Atp1a2*^{T345A} mice that had LFP recorded bilaterally from the cortex (n = 77 events) and cortex and hippocampus (n = 39 events).

SD in cortex	Proportion of total SD events	Hippocampal SD		Epileptiform burst
		Unilateral	Bilateral	
Bilateral	51% (39/77)	0% (0/39)	100% (39/39)	100% (39/39)
Unilateral	30% (23/77)	30% (7/23)	70% (16/23)	70% (16/23)
None	19% (15/77)	27% (4/15)	73% (11/15)	47% (7/15)

Spontaneous spreading depolarizations in *Atp1a2*^{T345A} mice exhibit a diurnal rhythm and preferentially initiate during sleep

Homozygous *Atp1a2*^{T345A} mice showed an average SD frequency of 0.95 ± 0.41 (range 0.47 – 2.2) SDs per day. The mean and median time between subsequent SDs was 26.4 and 24.7 h, respectively (Fig. 5A), suggesting that a diurnal pattern was present. Indeed, SDs were more likely to occur in the evening (Fig. 5B and C). Vigilance state analyses showed that mice were asleep immediately prior to 84% (128/153) of events, which was significantly more often than expected based on the average time animals were asleep over 24 h (51 ± 5%; $p < 0.01$, Grubbs' test). All animals were awake during the first minute after SD onset, with locomotor activity increasing from 13 ± 21% to 83 ± 13% (mean ± S.D.) during the minute preceding and following SD onset, respectively.

Since the majority of spontaneous SDs were preceded by LFP burst activity (139/153 events), we studied the animals' behavior during SDs in more detail. Seizure behavior occurred during 5% (8/153) of events (n = 7 with Racine stage 3, n = 1 with Racine stage 5) and only for events preceded by LFP burst activity. Following SD, body stretches, backward and sideward movements, body rotations and head turns and/or waving were observed in 90% (138/153) of events, in the first 4 minutes after SD onset. The most frequently observed SD-related behaviors were stretching (73%; 111/153 events), head waving (63%; 97/153 events) and body rotations (52%; 79/153 events), with stretching typically preceding body rotations and head waving.

FIGURE 5. Spontaneous spreading depolarizations (SDs) in homozygous *Atp1a2*^{T345A} mice occurred preferably during early hours of the dark period.

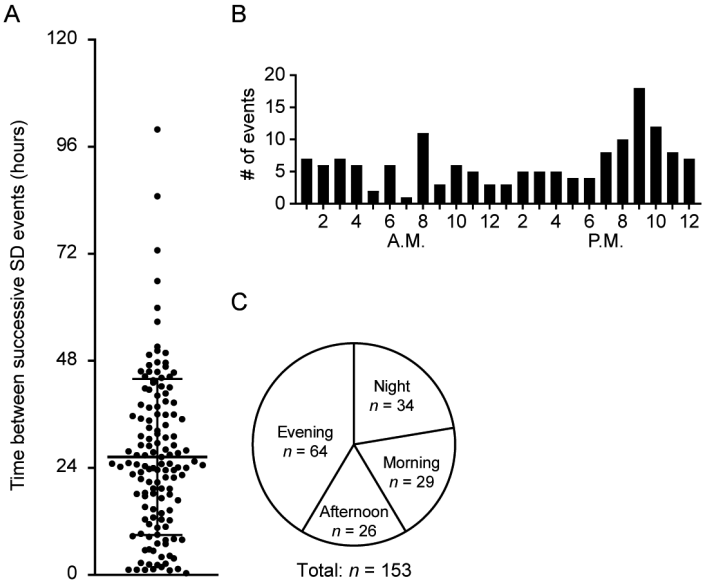

(A) Interval between spontaneous SD events in homozygous *Atp1a2*^{T345A} mice (n = 20, 2 – 10 days per animal). Each dot corresponds to a time interval between 2 successive SDs. **(B)** The distribution of spontaneous SD events during the day, counted per 1-h time bin. (C) SDs were more likely to occur in the evening ($\chi^2_{(3)} = 22.8$, $p < 0.001$).

Subregion-specific hippocampal hyperexcitability in homozygous *Atp1a2*^{T345A} mice

Interictal spikes occurred regularly in hippocampal CA1 and CA3 region in homozygous *Atp1a2*^{T345A} mice, specifically during NREM sleep. These high-amplitude spikes had only a low-amplitude correlate in the cortical LFP (Fig. 6A), suggesting a local origin. Since throughout development NKA activity is increased in CA3 when compared to CA1,[24] we tested whether the *Atp1a2*^{T345A} mutation affects SD susceptibility differently in these hippocampal areas. In the WT immature hippocampus, the CA3 region was previously shown to have a higher threshold for K^+-induced SD when compared to CA1.[25] To compare the SD susceptibility of the CA1 and CA3 in WT and homozygous *Atp1a2*^{T345A} mice, we electrically stimulated the ventral left CA3 region (1-ms bipolar pulses at 60 Hz for 2 s) while recording LFP in right CA1 and CA3 in the dorsal hippocampus. We observed Ads followed by SD in both WT (n = 9) and homozygous *Atp1a2*^{T345A} (n = 4) mice. However, a different pattern was observed for the various genotypes: CA3 SD followed CA1 SD in the majority (6/9) of WT mice, whereas it preceded CA1 SD in all homozygous *Atp1a2*^{T345A} mice (Fig. 6B). Similarly, CA3 SD preceded CA1 SD during 3 spontaneous events that were observed

in 3 of the 4 homozygous *Atp1a2*^{T345A} mice with implanted CA1 and CA3 electrodes (Fig. 6C). Irrespective of the hippocampal subregion, homozygous *Atp1a2*^{T345A} mice showed an increased duration of the negative DC-shift, when compared to WT mice (Fig. 6D). These data further support a role for hippocampal hyperexcitability in the phenotype of *Atp1a2*^{T345A} mice, affecting the CA3 subregion most evidently.

Atp1a2^{T345A} mice show decreased seizure propagation and reduced susceptibility to hippocampal kindling

Homozygous *Atp1a2*^{T345A} mice showed seizure-related behavior for only a small minority of the spontaneous SD events. We therefore evaluated whether seizure progression is affected in these animals. Stimulation of the left ventral hippocampus (1-ms bipolar pulses at 60 Hz for 2 s) resulted in Ads followed by SD in the right hippocampus of WT, heterozygous and homozygous *Atp1a2*^{T345A} mice (example traces in Fig. 7A), which propagated to the cortex in all (7/7) homozygous, a fraction (2/12) of heterozygous, and none (0/11) of the WT mice. The duration and power of the Ads in hippocampal LFP were comparable (Fig. 7B), but were both significantly reduced in V1 of both heterozygous and homozygous mutant mice, and more so for homozygous mutant mice (Fig. 7C). Moreover, whereas the threshold for eliciting Ads was comparable between the genotypes (Fig. 7D), postictal normalized LFP power in V1 was reduced in homozygous mutant when compared to WT mice (preceding SD arrival; Fig. 7E). Twice daily repetitive stimulation at the AD threshold current over the course of 15 days showed reduced seizure expression during kindling in heterozygous and homozygous mutants when compared to WT mice following stimulations 9 to 30, while seizure expression was significantly impaired in homozygous mutant when compared to heterozygous mutant mice following stimulations 18 to 30 (Fig. 7F).

FIGURE 6. Hippocampal hyperexcitability in homozygous *Atp1a2*^{T345A} mice disproportionately affects the CA3 region.

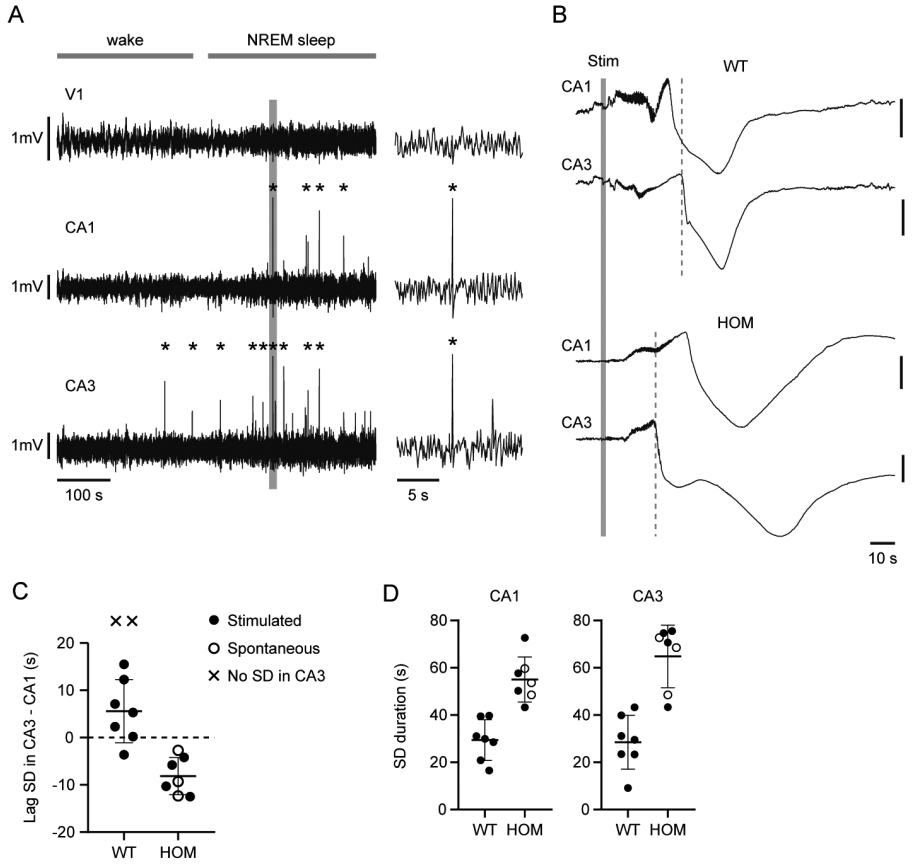

(A) Example LFP recordings in a homozygous *Atp1a2*^{T345A} mouse showing interictal spikes (indicated by asterisks) in hippocampal CA1 and CA3 during NREM sleep, that in the primary visual cortex (V1) was of similar amplitude as background activity. **(B)** Example DC signals from the right CA1 and CA3 region of a wildtype (WT, top) and homozygous *Atp1a2*^{T345A} mouse (HOM, bottom), showing afterdischarges followed by SD, after electrical stimulation (Stim) of the left CA3 region. Note the different spreading pattern of SD in the 2 genotypes: CA3 SD followed CA1 SD in the WT mouse, whereas it preceded CA1 SD in the homozygous *Atp1a2*^{T345A} mouse. Vertical scale bars indicate 10 mV. **(C)** Lag between SD initiation in CA3 *vs* CA1 (i.e. positive values indicate CA1 preceding CA3). In contrast to WT mice, in homozygous *Atp1a2*^{T345A} mice CA3 SD events are more likely to precede CA1 SD events ($p = 0.0012$, Mann-Whitney U test; data from stimulated and spontaneous SD events were grouped for *Atp1a2*^{T345A} mice; WT animals in which no CA3 SD occurred were excluded). **(D)** SD duration in both CA1 and CA3 was significantly greater for homozygous *Atp1a2*^{T345A} mice when compared to WT mice (both $p < 0.001$, Mann-Whitney U test; data from stimulated and spontaneous SD events were grouped for *Atp1a2*^{T345A} mice).

FIGURE 7. Seizure expression and kindling rates are decreased in *Atp1a2*^{T345A} mice.

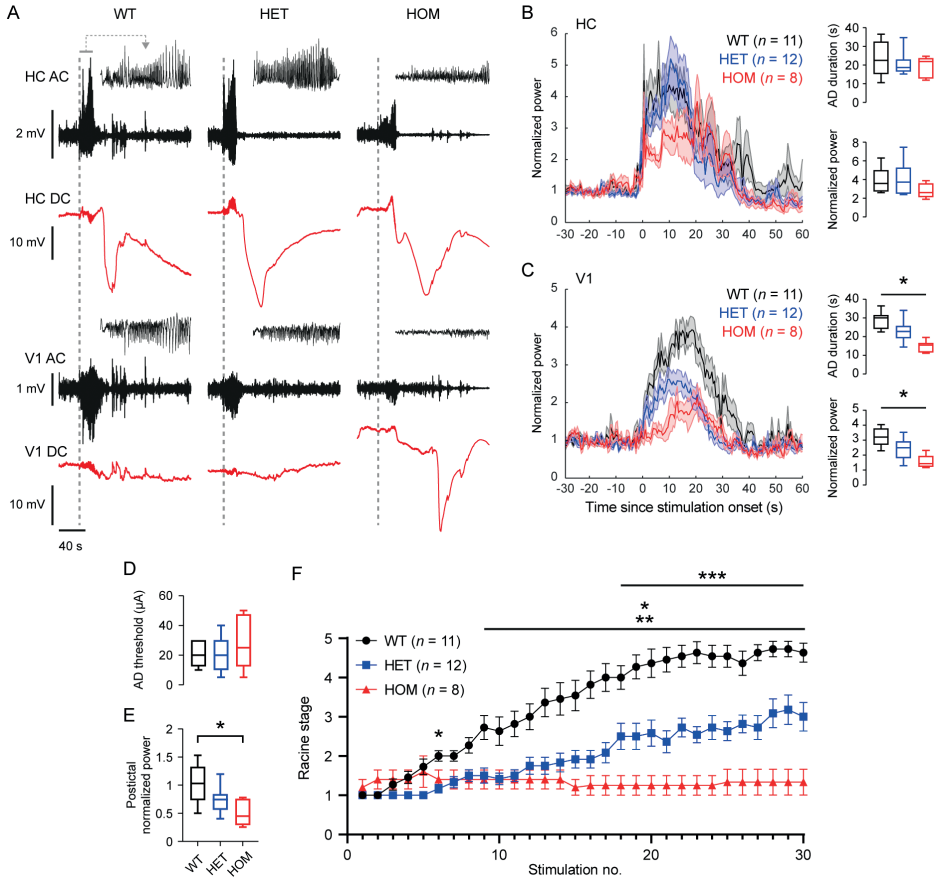

(A) Example LFP signals (AC in black, DC in red) obtained in right hippocampal CA3 (HC) and primary visual cortex (V1) following electrical stimulation of the left HC (dashed line) for wildtype (WT), heterozygous (HET) and homozygous (HOM) *Atp1a2*^{T345A} mice. Insets detail the first 20 s after stimulation. **(B)** Time series of HC LFP power normalized to baseline (30 s preceding stimulation) relative to stimulation onset (at $t = 0$ s). HC afterdischarge (AD) duration and power was similar across genotypes (*right*). **(C)** Time series of V1 LFP power normalized to baseline, demonstrating significant differences in V1 AD duration and power between all genotypes (*right*; $^*p < 0.01$; Welch's ANOVA test followed by unpaired *t* tests with Welch's correction). **(D)** AD threshold was comparable between genotypes ($p = 0.50$; Kruskal-Wallis test). **(E)** Postictal (i.e. after termination of the AD) HC LFP power was significantly reduced in HET and HOM mutant mice when compared to WT ($^*p = 0.047$, $^{**}p = 0.004$; Welch's ANOVA test followed by unpaired *t* tests with Welch's correction). **(F)** Seizure-related behavior, assessed using the Racine scale, during hippocampal kindling achieved by repetitive of stimulation of the HC at the AD threshold (twice daily for 15 days). Seizure-related behavior was decreased in mutant mice, showing a gene-dosage effect over the course of the kindling paradigm (*WT *vs* HET, **WT *vs* HOM, ***HET *vs* HOM; $p < 0.05$; two-way ANOVA with Tukey's multiple comparisons test).

Blockade of persistent sodium currents but not NMDA receptors limits hippocampal initiation of spontaneous spreading depolarizations in homozygous *Atp1a2*^{T345A} mice

Since spontaneous SD occurred regularly in homozygous *Atp1a2*^{T345A} mice, we next assessed whether these SDs could be pharmacologically modulated. NMDA receptor (NMDAR) antagonists, including the non-selective NMDAR antagonist MK801, are potent inhibitors of SD initiation.[26,27] We tested whether twice daily intraperitoneal injections with 0.5 mg/kg MK801, a dose that was previously shown to decrease the number of cortical SDs following cortical KCl application,[28] could decrease spontaneous hippocampal and cortical SD occurrence in homozygous *Atp1a2*^{T345A} mice. In 6 homozygous *Atp1a2*^{T345A} mice, 17 hippocampal SDs occurred over the course of 3 days of MK801 treatment, compared to 15 SDs during vehicle treatment. Cortical appearance of SD followed the majority of hippocampal SDs during vehicle treatment (13/15), but were effectively blocked by MK801 treatment (0/17; example trace in Fig. 8A), indicating effective suppression of SD propagation from hippocampus to cortex. However, MK801 failed to affect the number of spontaneous hippocampal SDs within the 3-day treatment period (Fig. 8B). In fact, MK801 tended to lead to a faster occurrence of an SD event after injection (range 480 – 50,150 s) when compared to vehicle (range 2670 – 50,350 s) (Fig. 8C). Since the dosage of MK801 required to block SD initiation may be higher for hippocampal regions,[29] we additionally tested repeated doses of 2.5 (10 injections in 2 mice), 3.5 (4 injections in 1 mouse) and 5.0 (1 injection in 1 mouse) mg/kg. These doses resulted in abnormal behavior of the animal (loss of posture, immobility) and even early death (4/15 injections). Following the majority of injections (10/15), a hippocampal SD occurred shortly after injection (Fig. 8C). Since the regime was not well tolerated in the mutant mice, no additional experiments with repeated high doses of MK801 were performed.

Decreased effectiveness of NMDAR antagonism in SD initiation may be explained by increased extracellular K^+,[30] which could also ignite SD in the hippocampus by a positive feedback loop involving K^+-induced increases in persistent sodium currents.[31] We therefore tested whether treatment with GS967, a preferential inhibitor of persistent sodium currents, affected SD occurrence in *Atp1a2*^{T345A} mice (n = 8). After one week of baseline recordings, standard chow was replaced by chow containing GS967 (8 mg/kg of chow, estimated to result in a daily dose of 1.5 mg/kg[21]) for one week, again replaced by standard chow for one week of recovery (Fig. 8D). The number of spontaneous hippocampal SD events decreased during GS967 treatment (Fig. 8E). However, GS967 did not prevent spread of SD to the cortex (cortical SD in 15/15 events, compared to 60/65 events during baseline/recovery, $\chi^2_{(1)} = 1.1$, $p < 0.267$) nor did the compound affect the time delay between hippocampal and V1 SD (61 ± 21 s during GS967 treatment vs 66 ± 28 s during baseline; $p = 0.56$). These data suggest that persistent sodium currents but not NMDAR-mediated currents contribute to spontaneous hippocampal SD initiation in homozygous *Atp1a2*^{T345A} mice.

FIGURE 8. Blockade of persistent sodium currents, but not NMDA receptor antagonism, decreased initiation of spontaneous SDs in homozygous *Atp1a2*^{T345A} mice.

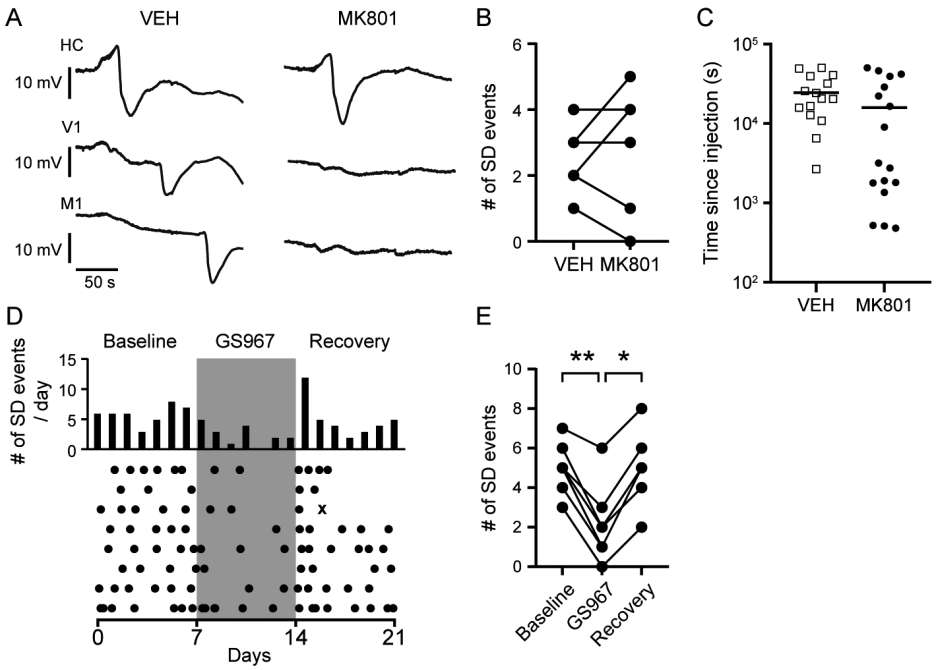

(A) Example LFP DC recordings in hippocampus (HC), primary visual cortex (V1) and primary motor cortex (M1) of a homozygous *Atp1a2*^{T345A} mouse during treatment with vehicle (VEH) or MK801 (0.5 mg/kg, twice daily over the course of 3 days). **(B)** Although MK801 did prevent SD propagation to cortex, it did not affect spontaneous hippocampal event rate ($n = 8$; $p = 0.50$, Wilcoxon signed-rank test). **(C)** Time between injection of 0.5 m/kg MK801 or vehicle and the first hippocampal SD ($p = 0.0637$, Mann-Whitney U test). Following MK801, no propagation to the cortex was observed. **(D)** Raster plot with dots indicating spontaneous hippocampal SD events in homozygous *Atp1a2*^{T345A} mice ($n = 8$) while fed standard chow (baseline and recovery) or GS967-compounded chow (shaded area); superimposed a histogram showing the total event count per 24 h. Note that one animal died during the 21-day recording period, indicated by a cross. **(E)** Spontaneous SD events in homozygous *Atp1a2*^{T345A} mice were significantly less likely to occur during GS967 treatment (*$p = 0.016$ and **$p = 0.008$, Wilcoxon signed-rank rest; $n = 7$; the animal that died during the recovery period was not included in the analysis).

DISCUSSION

In this study, we present a novel FHM2 knock-in mouse model with the *Atp1a2*^{T345A} mutation. Homozygous mutant mice are viable and demonstrate regular spontaneous SD. SD events typically originated from the hippocampus and propagated to the visual cortex and then in a caudal-to-rostral pattern. Hippocampal PO_2 measurements indicated that the spontaneous SD events were not caused by hypoxia. Heterozygous mutant mice rarely exhibit spontaneous SD. Whereas heterozygotes only show an increased propagation speed of electrically evoked cortical SD, homozygotes also show a decreased threshold for such events. Hence, whereas the heterozygous *Atp1a2*^{T345A} mice show certain features relevant to patients, who have one mutant gene copy, the homozygotes provide the unique opportunity to investigate spontaneous SD events. Inhibition of persistent sodium currents reduced the occurrence of spontaneous SD in homozygotes, without affecting SD propagation. Notably, NMDAR antagonism did not inhibit hippocampal SD initiation but blocked subsequent appearance of SD in the cortex in homozygotes. These findings indicate that modelling spontaneous SD allows differentiation of its initiation and propagation mechanisms, potentially impacting treatment strategies.

Spontaneous SDs have not been reported in existing FHM2 mouse models including the *Atp1a2*^{W887R} [5, 7, 32] and *Atp1a2*^{G301R} [23] strains. Homozygous mice of these mouse strains die at birth, similar to *Atp1a2*$^{-/-}$ mice.[4, 33] In the present study, homozygous *Atp1a2*^{T345A} mice show a normal expression level of α_2NKA protein. The location of the T345A missense mutation on the cytoplasmic stalk domain adjacent to transmembrane segment 4 suggests it would affect Na^+/K^+ ATPase functioning. Cellular studies have shown different consequences of the T345A mutation including decreased K^+ affinity,[16] lower maximum turnover rate,[14] or even preserved Na^+/K^+ATPase functioning for the parameters tested.[15] In contrast, the W887R[16] and G301R[17] mutants fail to show any ATPase activity and do not support cell growth. Thus, available data reflect the phenotype of *Atp1a2* mutants, with *Atp1a2*^{T345A} being the mildest. A gene dosage effect for the T345A mutation was evidenced by a relatively high incidence of spontaneous SDs and decreased electrical threshold for induced SDs, in homozygous *versus* heterozygous *Atp1a2*^{T345A} mice. Comparison of results from heterozygous *Atp1a2*^{T345A} mice with *in vivo* SD susceptibility data of heterozygous mutants from published FHM2 mouse models[5, 6, 32, 34] remains qualitative as a direct comparison is hampered by differences in methodology, including differences in SD induction methods (e.g. electrical stimulation and KCl) and brain state during these experiments (i.e. awake freely behaving in our study, versus anesthetized or head-fixed awake in studies in other models). Nevertheless, the enhanced susceptibility to evoked cortical SDs in heterozygous and homozygous *Atp1a2*^{T345A} mice underscores the role of astrocytic buffering in SD susceptibility in the context of FHM2, as nicely illustrated for mice of the *Atp1a2*^{W887R} strain by reduced rates of clearance of glutamate and K^+ by cortical astrocytes during neuronal activity.[7, 32] The observation of sudden apnea preceding early mortality in homozygous *Atp1a2*^{T345A} mice suggests that besides in the hippocampus, local or spreading depolarizations may also occur in the brainstem, as was demonstrated in FHM1[35, 36]

and FHM3[37] mouse models. Regardless, the high incidence and regularity of spontaneous SDs in homozygous *Atp1a2*^{T345A} mice is especially of interest to advance the study of mechanisms and consequences of SD initiation.

In all homozygous *Atp1a2*^{T345A} mice studied, spontaneous SD events were recorded. SD events showed a diurnal rhythm and preferably initiated during sleep. Clinical studies have demonstrated a similar circadian periodicity in attacks both for migraine with and without aura, with attacks occurring preferably during the early morning,[38, 39] although peaks at the middle of the day have also been reported.[40] The majority of patients report migraine attacks upon awakening,[41] which we also observed for homozygous *Atp1a2*^{T345A} mice. Astrocytic activity contributes to the transition from sleep to wakefulness.[42] Considering the role of astrocytes in K^+ clearance and the changes in brain extracellular K^+ levels over the sleep-wake cycle,[43-45] sudden surges in extracellular K^+ during the sleep-wake transition may facilitate SD initiation.

A majority of hippocampal SDs in homozygous *Atp1a2*^{T345A} mice was preceded by epileptiform bursts of relatively short duration and moderate amplitude. The typical observation of hippocampal burst activity followed by SD in homozygous *Atp1a2*^{T345A} mice is in line with preclinical and modeling data showing that SD can initiate from a short localized burst of network activity[46, 47] (for reviews see Somjen 2001[1]; Ayata and Lauritzen 2015[48]). The observation that the amplitude of the epileptiform bursts was always higher in hippocampus compared to cortex, seems further support of a hippocampal origin of the events. Notably, overt seizure-related behavior was absent during most of the spontaneous events, while both heterozygous and homozygous *Atp1a2*^{T345A} mice displayed decreased hippocampal kindling. Such inverse relationship between epileptic kindling and SD incidence has been reported previously.[49] The start of the burst activity preceded hippocampal SD by tens of seconds, which would allow sufficient time for seizure activity to spread and cause seizure-related behaviors. Indeed, in wildtype mice hippocampal SD also occurred during kindling experiments, and it was already preceded by epileptic activity in both LFP and behavior. We thus consider it less likely that reduced seizure expression in *Atp1a2*^{T345A} mice is mediated by the suppressive effects of SD. Previous work has shown that seizure propagation relies on connectivity and synaptic transmission.[50, 51] We thus hypothesize that the decreased amplitudes and duration of ADs in the cortex of *Atp1a2*^{T345A} mice result from less efficient synaptic and/or electric field transmission in these mice, which could hamper seizure generalization.

Impaired glutamate uptake resulting in activation of NMDARs has been shown a critical mechanism underlying SD initiation in *Atp1a2*^{W887R} mice.[7, 32] Such facilitation of cortical SD has been attributed to impaired glutamate clearance by cortical astrocytes, indicating that astrocytic α_2NKA regulates glutamate uptake through coupling with glutamate transporters.[7] Although various studies report that blocking NMDARs effectively blocks experimentally induced SD (for reviews see Klass et al., 2018[27]; Telles et al., 2021), it remains unclear whether this effect is caused by inhibition of SD initiation or propagation mechanisms, or both.[29] Contrasting conclusions may arise from the location of recordings relative to the SD initiation site, for example when comparing the role of NMDARs in hippocampal SD[52] *versus* cortical SD.[53] Alternatively, SD initiation mechanisms

(and related susceptibility to NMDAR modulation) may differ across brain regions and animal models, and might also be influenced by the experimental approach, including the choice for *in vivo* (under anesthesia or awake) or *ex vivo* experimentation. For example, blocking NMDARs did not prevent KCl-induced SD onset in the hippocampus of anesthetized rats,[54] contrasting various reports of suppressing effects of NMDAR blockers on cortical SD, either induced by KCl in cortical slices,[53, 55, 56] by KCl or electrical stimulation in anesthetized mice[28] or rats,[26, 57-60] or by optogenetics in awake mice.[61] Overall, SD initiation mechanisms may be ideally studied in disease models where they occur spontaneously, in the absence of anesthesia. Here, MK801 (0.5 mg/kg i.p.) failed to decrease the frequency of spontaneous hippocampal SDs in homozygous *Atp1a2*^{T345A} mice, while preventing appearance in cortex. While high doses (2.5 – 5.0 mg/kg i.p.) of MK801 were not well tolerated, especially not in homozygous mutants, hippocampal SDs were still observed, albeit without subsequent SD appearance in cortex. The abnormal behaviors (loss of posture and immobility) and even early mortality observed in homozygous *Atp1a2*^{T345A} mice following high doses MK801 expand findings of locomotor abnormalities including immobility, ataxia and stereotypic behaviors following high doses systemic administration of MK801 in wildtype mice and rats[62-64] that may warrant some caution when interpreting brain activity, including that of SD following high dosage MK801 under awake conditions. Regardless, our observations with both low and high doses of MK801 suggest reduced sensitivity of homozygous *Atp1a2*^{T345A} mice to NMDAR blockade, at least in the context of spontaneous hippocampal SD initiation. Conversely, the persistent sodium current blocker GS967 did suppress hippocampal SD occurrence, while propagation to cortical regions was not impaired, suggesting that action potential generation is critical for initiation but perhaps not so much for propagation of spontaneous SDs in homozygous *Atp1a2*^{T345A} mice. Our data complement earlier findings from anesthetized rats that showed a small effect of GS967 on increasing the threshold of electrically evoked CSD,[65] suggesting that in the absence of intrinsic hyperexcitability, the role of persistent sodium currents for SD initiation is only modest. Our results may be explained by a (general or transient) increase in brain extracellular K^+ in *Atp1a2*^{T345A} mice, which is expected to decrease the effectiveness of NMDAR antagonists,[30] although this was not demonstrated, while increasing persistent sodium currents.[31] As such, our data suggest that targeting persistent sodium currents, in addition to NMDAR modulation, may be a promising treatment strategy in FHM2, likely depending on the mutation, and which may also be applicable to other SD-related diseases.

Acknowledgements

This work was supported by the Dutch National Epilepsy Foundation (2017-10 to and A.M.J.M.v.d.M., the European Innovation Council EIC Pathfinder Programme Project MICROVASC (no 101070917 to A.M.J.M.v.d.M.), European Union Joint Programme – Neurodegenerative Disease Research project REBALANCE (no 10510062210003 to E.A.T and A.M.J.M.v.d.M.) and the Medical Delta program "Medical NeuroDelta: Ambulant Neuromonitoring for Prevention and Treatment of Brain Disease" (to A.M.J.M.v.d.M.). We thank Praxis Precision Medicines for providing PRAX-330-modified chow and Kris Kahlig for input on the related experiments.

REFERENCES

1. Somjen, G.G., Mechanisms of spreading depression and hypoxic spreading depression-like depolarization. *Physiol Rev*, 2001. 81(3): p. 1065-96.
2. Lauritzen, M., et al., Clinical relevance of cortical spreading depression in neurological disorders: migraine, malignant stroke, subarachnoid and intracranial hemorrhage, and traumatic brain injury. *J Cereb Blood Flow Metab*, 2011. 31(1): p. 17-35.
3. De Fusco, M., et al., Haploinsufficiency of ATP1A2 encoding the Na+/K+ pump alpha2 subunit associated with familial hemiplegic migraine type 2. *Nat Genet*, 2003. 33(2): p. 192-6.
4. Moseley, A.E., et al., The Na,K-ATPase alpha 2 isoform is expressed in neurons, and its absence disrupts neuronal activity in newborn mice. *J Biol Chem*, 2003. 278(7): p. 5317-24.
5. Leo, L., et al., Increased susceptibility to cortical spreading depression in the mouse model of familial hemiplegic migraine type 2. *PLoS Genet*, 2011. 7(6): p. e1002129.
6. Kros, L., K. Lykke-Hartmann, and K. Khodakhah, Increased susceptibility to cortical spreading depression and epileptiform activity in a mouse model for FHM2. *Sci Rep*, 2018. 8(1): p. 16959.
7. Capuani, C., et al., Defective glutamate and K+ clearance by cortical astrocytes in familial hemiplegic migraine type 2. *EMBO Mol Med*, 2016. 8(8): p. 967-86.
8. Sugimoto, H., et al., Astrocytes in Atp1a2-deficient heterozygous mice exhibit hyperactivity after induction of cortical spreading depression. *FEBS Open Bio*, 2020. 10(6): p. 1031-1043.
9. Reiffurth, C., et al., Na(+)/K(+)-ATPase alpha isoform deficiency results in distinct spreading depolarization phenotypes. *J Cereb Blood Flow Metab*, 2020. 40(3): p. 622-638.
10. James, P.F., et al., Identification of a specific role for the Na,K-ATPase alpha 2 isoform as a regulator of calcium in the heart. *Mol Cell*, 1999. 3(5): p. 555-63.
11. Chatron, N., et al., A novel lethal recognizable polymicrogyric syndrome caused by ATP1A2 homozygous truncating variants. *Brain*, 2019. 142(11): p. 3367-3374.
12. Monteiro, F.P., et al., Biallelic loss of function variants in ATP1A2 cause hydrops fetalis, microcephaly, arthrogryposis and extensive cortical malformations. *Eur J Med Genet*, 2020. 63(1): p. 103624.
13. Segall, L., et al., Kinetic alterations due to a missense mutation in the Na,K-ATPase alpha2 subunit cause familial hemiplegic migraine type 2. *J Biol Chem*, 2004. 279(42): p. 43692-6.
14. Schack, V.R., R. Holm, and B. Vilsen, Inhibition of phosphorylation of na+,k+-ATPase by mutations causing familial hemiplegic migraine. *J Biol Chem*, 2012. 287(3): p. 2191-202.
15. Weigand, K.M., et al., Biochemical characterization of sporadic/familial hemiplegic migraine mutations. *Biochim Biophys Acta*, 2014. 1838(7): p. 1693-700.
16. Segall, L., et al., Alterations in the alpha2 isoform of Na,K-ATPase associated with familial hemiplegic migraine type 2. *Proc Natl Acad Sci U S A*, 2005. 102(31): p. 11106-11.
17. Tavraz, N.N., et al., Impaired plasma membrane targeting or protein stability by certain ATP1A2 mutations identified in sporadic or familial hemiplegic migraine. *Channels (Austin)*, 2009. 3(2): p. 82-7.
18. Pettitt, S.J., et al., Agouti C57BL/6N embryonic stem cells for mouse genetic resources. *Nat Methods*, 2009. 6(7): p. 493-5.

19. McAfee, S.S., et al., Minimally invasive highly precise monitoring of respiratory rhythm in the mouse using an epithelial temperature probe. *J Neurosci Methods*, 2016. 263: p. 89-94.
20. Jansen, N.A., et al., First FHM3 mouse model shows spontaneous cortical spreading depolarizations. *Ann Clin Transl Neurol*, 2020. 7(1): p. 132-138.
21. Baker, E.M., et al., The novel sodium channel modulator GS-458967 (GS967) is an effective treatment in a mouse model of SCN8A encephalopathy. *Epilepsia*, 2018. 59(6): p. 1166-1176.
22. Jansen, N.A., et al., Impaired theta-gamma Coupling Indicates Inhibitory Dysfunction and Seizure Risk in a Dravet Syndrome Mouse Model. *J Neurosci*, 2021. 41(3): p. 524-537.
23. Bottger, P., et al., Glutamate-system defects behind psychiatric manifestations in a familial hemiplegic migraine type 2 disease-mutation mouse model. *Sci Rep*, 2016. 6: p. 22047.
24. Haglund, M.M., et al., Developmental and regional differences in the localization of Na,K-ATPase activity in the rabbit hippocampus. *Brain Res*, 1985. 343(1): p. 198-203.
25. Haglund, M.M. and P.A. Schwartzkroin, Role of Na-K pump potassium regulation and IPSPs in seizures and spreading depression in immature rabbit hippocampal slices. *J Neurophysiol*, 1990. 63(2): p. 225-39.
26. Marrannes, R., et al., Evidence for a role of the N-methyl-D-aspartate (NMDA) receptor in cortical spreading depression in the rat. *Brain Res*, 1988. 457(2): p. 226-40.
27. Klass, A., R. Sanchez-Porras, and E. Santos, Systematic review of the pharmacological agents that have been tested against spreading depolarizations. *J Cereb Blood Flow Metab*, 2018. 38(7): p. 1149-1179.
28. Dhir, A., C. Lossin, and M.A. Rogawski, Propofol hemisuccinate suppresses cortical spreading depression. *Neurosci Lett*, 2012. 514(1): p. 67-70.
29. Pietrobon, D. and M.A. Moskowitz, Chaos and commotion in the wake of cortical spreading depression and spreading depolarizations. *Nat Rev Neurosci*, 2014. 15(6): p. 379-93.
30. Petzold, G.C., et al., Increased extracellular K+ concentration reduces the efficacy of N-methyl-D-aspartate receptor antagonists to block spreading depression-like depolarizations and spreading ischemia. *Stroke*, 2005. 36(6): p. 1270-7.
31. Somjen, G.G. and M. Muller, Potassium-induced enhancement of persistent inward current in hippocampal neurons in isolation and in tissue slices. *Brain Res*, 2000. 885(1): p. 102-10.
32. Parker, P.D., et al., Non-canonical glutamate signaling in a genetic model of migraine with aura. *Neuron*, 2021. 109(4): p. 611-628 e8.
33. Ikeda, K., et al., Malfunction of respiratory-related neuronal activity in Na+, K+-ATPase alpha2 subunit-deficient mice is attributable to abnormal Cl- homeostasis in brainstem neurons. *J Neurosci*, 2004. 24(47): p. 10693-701.
34. Tang, C., et al., Characteristics of cortical spreading depression and c-Fos expression in transgenic mice having a mutation associated with familial hemiplegic migraine 2. *Cephalalgia*, 2020. 40(11): p. 1177-1190.
35. Loonen, I.C.M., et al., Brainstem spreading depolarization and cortical dynamics during fatal seizures in Cacna1a S218L mice. *Brain*, 2019. 142(2): p. 412-425.
36. Jansen, N.A., et al., Apnea associated with brainstem seizures in Cacna1a (S218L) mice is caused by medullary spreading depolarization. *J Neurosci*, 2019. 39(48): p. 9633-9644.

37. Jansen, N.A., et al., Brainstem depolarization-induced lethal apnea associated with gain-of-function SCN1A(L263V) is prevented by sodium channel blockade. *Proc Natl Acad Sci U S A*, 2024. 121(14): p. e2309000121.
38. Fox, A.W. and R.L. Davis, Migraine chronobiology. Headache, 1998. 38(6): p. 436-41.
39. van Oosterhout, W., et al., Chronotypes and circadian timing in migraine. Cephalalgia, 2018. 38(4): p. 617-625.
40. Alstadhaug, K., R. Salvesen, and S. Bekkelund, 24-hour distribution of migraine attacks. *Headache*, 2008. 48(1): p. 95-100.
41. Kelman, L. and J.C. Rains, Headache and sleep: examination of sleep patterns and complaints in a large clinical sample of migraineurs. *Headache*, 2005. 45(7): p. 904-10.
42. Bojarskaite, L., et al., Astrocytic Ca(2+) signaling is reduced during sleep and is involved in the regulation of slow wave sleep. Nat Commun, 2020. 11(1): p. 3240.
43. Rasmussen, R., et al., Cortex-wide changes in extracellular potassium ions parallel brain state transitions in awake behaving mice. Cell reports, 2019. 28(5): p. 1182-1194. e4.
44. Ding, F., et al., Changes in the composition of brain interstitial ions control the sleep-wake cycle. *Science*, 2016. 352(6285): p. 550-555.
45. Rasmussen, R., M.H. Jensen, and M.L. Heltberg, Chaotic Dynamics Mediate Brain State Transitions, Driven by Changes in Extracellular Ion Concentrations. *Cell Syst*, 2017. 5(6): p. 591-603 e4.
46. Larrosa, B., et al., A role for glutamate and glia in the fast network oscillations preceding spreading depression. *Neuroscience*, 2006. 141(2): p. 1057-1068.
47. Wei, Y., G. Ullah, and S.J. Schiff, Unification of neuronal spikes, seizures, and spreading depression. *J Neurosci*, 2014. 34(35): p. 11733-43.
48. Ayata, C. and M. Lauritzen, Spreading Depression, Spreading Depolarizations, and the Cerebral Vasculature. *Physiol Rev*, 2015. 95(3): p. 953-93.
49. Koroleva, V.I., L.V. Vinogradova, and J. Bures, Reduced incidence of cortical spreading depression in the course of pentylenetetrazol kindling in rats. *Brain Res*, 1993. 608(1): p. 107-14.
50. Rossi, L.F., et al., Focal cortical seizures start as standing waves and propagate respecting homotopic connectivity. *Nat Commun*, 2017. 8(1): p. 217.
51. Choy, M., et al., Repeated hippocampal seizures lead to brain-wide reorganization of circuits and seizure propagation pathways. *Neuron*, 2021.
52. Mei, Y.Y., et al., NMDA receptors sustain but do not initiate neuronal depolarization in spreading depolarization. *Neurobiol Dis*, 2020. 145: p. 105071.
53. Vitale, M., et al., Mechanisms of initiation of cortical spreading depression. *J Headache Pain*, 2023. 24(1): p. 105.
54. Herreras, O., et al., Role of neuronal synchronizing mechanisms in the propagation of spreading depression in the in vivo hippocampus. *J Neurosci*, 1994. 14(11 Pt 2): p. 7087-98.
55. Anderson, T.R. and R.D. Andrew, Spreading depression: imaging and blockade in the rat neocortical brain slice. *J Neurophysiol*, 2002. 88(5): p. 2713-25.

56. Tottene, A., A. Urbani, and D. Pietrobon, Role of different voltage-gated Ca2+ channels in cortical spreading depression: specific requirement of P/Q-type Ca2+ channels. *Channels (Austin)*, 2011. 5(2): p. 110-4.
57. Willette, R.N., P.G. Lysko, and C.F. Sauermelch, A comparison of (+)SK&F 10047 and MK-801 on cortical spreading depression. *Brain Res*, 1994. 648(2): p. 347-51.
58. Lauritzen, M. and A.J. Hansen, The effect of glutamate receptor blockade on anoxic depolarization and cortical spreading depression. *J Cereb Blood Flow Metab*, 1992. 12(2): p. 223-9.
59. Menniti, F.S., et al., CP-101,606, an NR2B subunit selective NMDA receptor antagonist, inhibits NMDA and injury induced c-fos expression and cortical spreading depression in rodents. *Neuropharmacology*, 2000. 39(7): p. 1147-55.
60. Peeters, M., et al., Effects of pan- and subtype-selective N-methyl-D-aspartate receptor antagonists on cortical spreading depression in the rat: therapeutic potential for migraine. *J Pharmacol Exp Ther*, 2007. 321(2): p. 564-72.
61. Masvidal-Codina, E., et al., Characterization of optogenetically-induced cortical spreading depression in awake mice using graphene micro-transistor arrays. *J Neural Eng*, 2021. 18(5).
62. Tricklebank, M.D., et al., The behavioural effects of MK-801: a comparison with antagonists acting non-competitively and competitively at the NMDA receptor. *Eur J Pharmacol*, 1989. 167(1): p. 127-35.
63. Deutsch, S.I., R.B. Rosse, and J. Mastropaolo, Behavioral approaches to the functional assessment of NMDA-mediated neural transmission in intact mice. *Clin Neuropharmacol*, 1997. 20(5): p. 375-84.
64. Wu, J., et al., Bimodal effects of MK-801 on locomotion and stereotypy in C57BL/6 mice. *Psychopharmacology (Berl)*, 2005. 177(3): p. 256-63.
65. Morais, A., et al., Inhibition of persistent sodium current reduces spreading depression-evoked allodynia in a mouse model of migraine with aura. *Pain*, 2023. 164(11): p. 2564-2571.

SUPPLEMENTARY MATERIAL

FIGURE S1. Homozygous *Atp1a2*^{T345A} mice showed a reduced body weight development and normal behavioral activity levels.

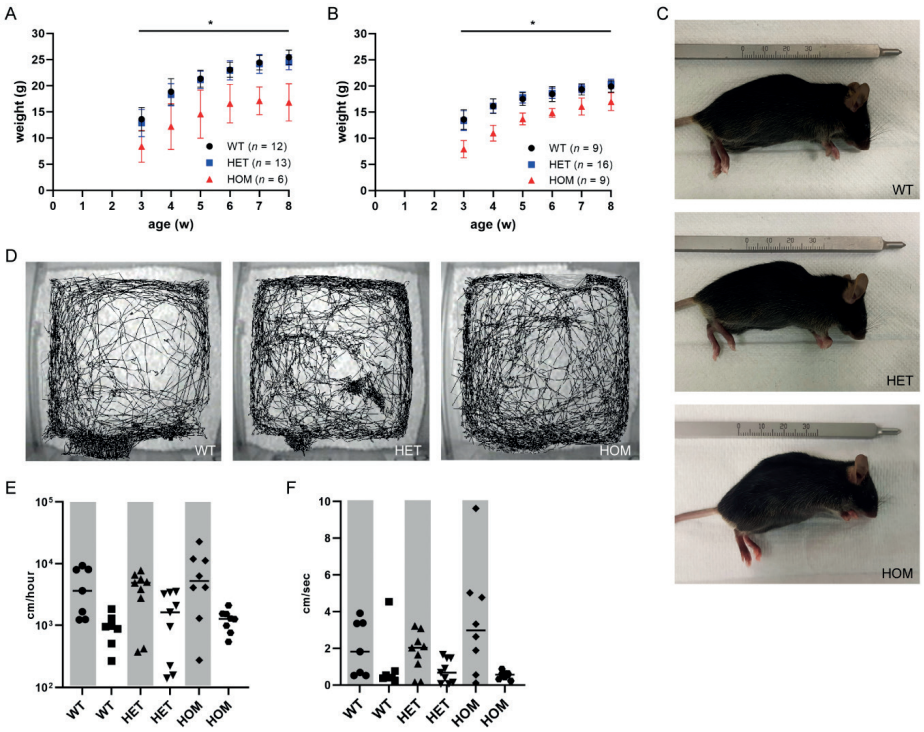

Both male **(A)** and female **(B)** homozygous (HOM), but not heterozygous (HET), *Atp1a2*^{T345A} mice showed reduced body weight (*$p < 0.01$, for WT versus HOM mice) and size (examples in **C**). **(D)** Representative tracking results (45 min, during the dark phase) from a WT, heterozygous and homozygous *Atp1a2*^{T345A} mouse. Total distance moved **(E)** and mean velocity **(F)** did not indicate differences in behavioral activity levels in WT, heterozygous or homozygous *Atp1a2*^{T345A} mice. Analyses from light and the dark periods are indicated by white and gray background, respectively.

FIGURE S2. Example of burst activity preceding SD in a homozygous *Atp1a2*^{T345A} mouse.

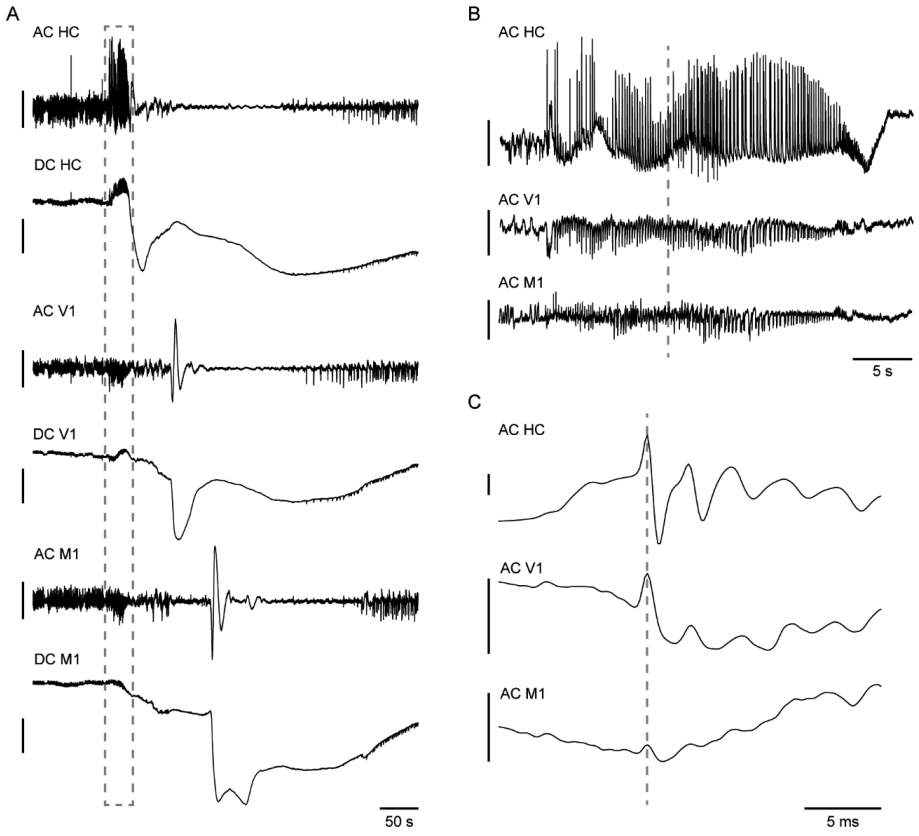

(A) Hippocampal (HC), primary visual cortex (V1) and primary motor cortex (M1) AC and DC LFP recordings during a burst (dashed box, detailed in B) followed by spontaneous SD in a homozygous *Atp1a2*^{T345A} mouse. **(B)** Burst activity amplitude was most pronounced in HC LFP, with high-amplitude spikes (example indicated by dashed line, detailed in **C**) synchronizing with lower amplitude spikes in V1 and M1. Vertical scale bars indicate 2 mV (AC) and 10 mV (DC) for **A** and **B**, and 1 mV for **C**

FIGURE S3. Example of a hippocampal partial oxygen pressure (PO2) recording during spontaneous SD in a homozygous *Atp1a2*^{T345A} mouse.

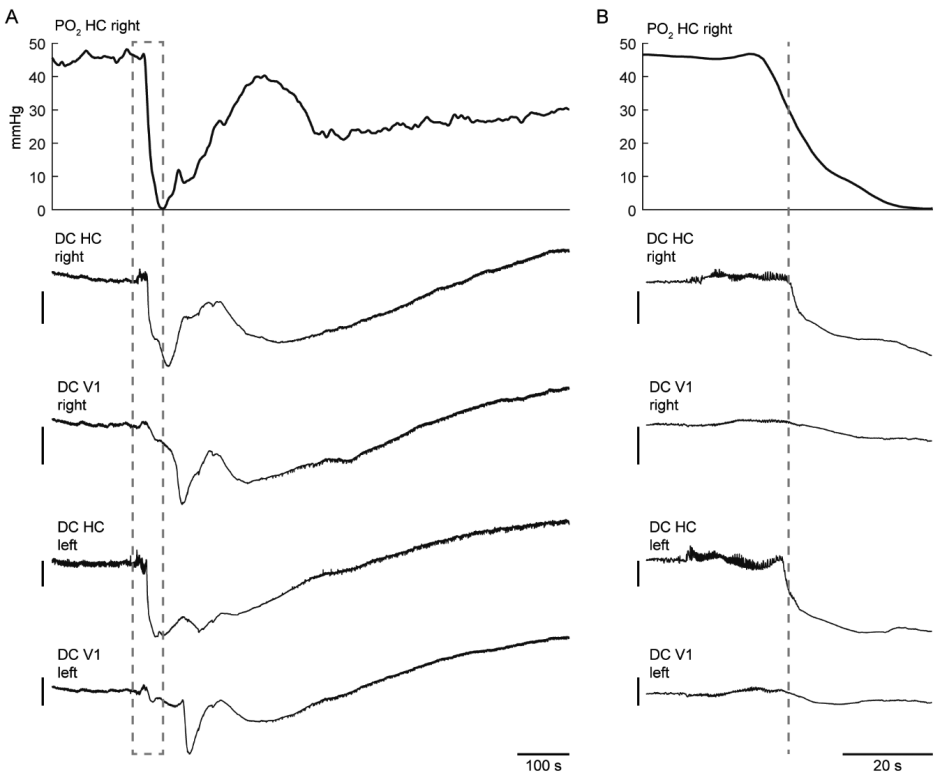

(A) Hippocampal (HC) PO_2 decreased during burst activity (dashed box, detailed in **B**) and the subsequent SD as depicted by the HC DC signal (ipsilateral onset indicated by a dashed line in **B**), preceding SD in the primary visual cortex (V1). Note that HC PO_2 was within normoxic range (>18 mmHg) at the onset of the DC shift. Vertical scale bars indicate 10 mV.